ESCUELA TÉCNICA SUPERIOR DE INGENIEROS INDUSTRIALES Y DE TELECOMUNICACIÓN

UNIVERSIDAD DE CANTABRIA

Trabajo Fin de Grado

Electrochemical characterisation of bimetallic materials for CO_2 reduction

Para acceder al Título de

Graduado en Ingeniería Química

Autor: Stanislav Shaklein
Fecha: Octubre 2017

Abstract

The growth of CO_2 concentration in the atmosphere is leading to an increasing global warming concern. Among the different approaches to reduce CO_2 emissions, the application of Carbon Capture and Utilisation technologies is particularly interesting because our reliance on fossil fuels can be reduced, producing also value added chemicals. There are several methods to activate and convert CO_2 into useful chemicals. The electrochemical reduction option seems to be one of the most interesting possibilities owing to the opportunity to carry out the CO_2 reduction reaction at ambient conditions. However, there are some issues that limit the practical application of this technology in the short-term: catalytic materials (involving lower activities, selectivities and stabilities) and mass transfer limitations issues. Therefore, the aim of this work is to prepare and characterise electrochemically gas diffusion electrodes based on bimetallic materials (Cu-Au, Cu-Mo, Cu-Ru and Cu-Pd) and bimetallic Metal Organic Frameworks (HKUST-1, HPd10, HZn10, HRu10, HBi5, HBi20, HBi10mix and CAU-17) that could be able to reduce reaction overpotentials and adsorption of reaction intermediates in the CO_2 reduction to methanol.

The working electrodes were manufactured by air-brushing a microporous layer based on carbon black powder (2.6 mg/cm^2) onto a carbon paper support. Then, different catalytic layers were airbrushed on it at different catalytic loadings (i.e. 0.5, 1 and 2 mg/cm^2). The final bimetallic electrodes were characterised by cyclic voltammetry and Tafel plot analyses. The effect of the catalytic loading showed the highest activity for Cu-Pd-based electrodes at the 2 mg/cm^2 loading, although only slight differences in activity can be observed between the electrodes tested. Higher catalytic activities were observed under N_2 conditions due to the effect of the hydrogen evolution reaction, competing with CO_2 conversion in the presence of this gas. Comparing the current-voltage responses, Cu-Pd electrodes showed the highest catalytic activity (-21 mA/cm^2) at 1 mg/cm^2. The most active Metal Organic Framework was HBi5 (5 wt% of Bi in HKUST-1, composed of Cu), which was interestingly stable after 40 cycles. Tafel plot analyses showed differences in the slopes for the activation of CO_2 at Cu-Pd, Cu and HBi5 materials. The lowest kinetic barrier for this step was achieved at Cu-Pd-based electrodes (83.7 mV/dec).

The most active bimetallic and Metal Organic Framework materials were compared with Cu electrodes. In general, bimetallic electrodes showed higher activities than the bimetallic Metal Organic Framework-based electrodes tested, and in particular Cu-Pd-based electrodes were able to surpass activity values achieved with Cu. Thus, Cu-Pd-based electrodes seem to be interesting for CO_2 electroreduction processes, even though further electrochemical cell tests are needed to analyse the selectivity, productivity and efficiency of these materials for the continuous CO_2 electroreduction.

Acknowledgments

I would like to thank the University of Cantabria for these 3 months that I spent in Santander. It was a great experience and big pleasure to make my final project here.

I also want to acknowledge my supervisors Iván Merino García and Jonathan Albo Sánchez for supporting and guiding me during the whole period of the project.

I would also like to thank to my supervisor in Israel Ariela Burg for helping and supporting me in my project the whole time.

Table of contents

Figures:

1 Introduction

The large consumption of fuels as a source of energy as well as the increased energy demand in the last century has led to a rise in the concentration of carbon dioxide (CO_2) into the atmosphere. Nowadays, this concentration is higher than 400 ppm [1] and this value is increasing by approximately 2 ppm each year [2]. Figure 1 shows concentration of CO_2 along period of time.

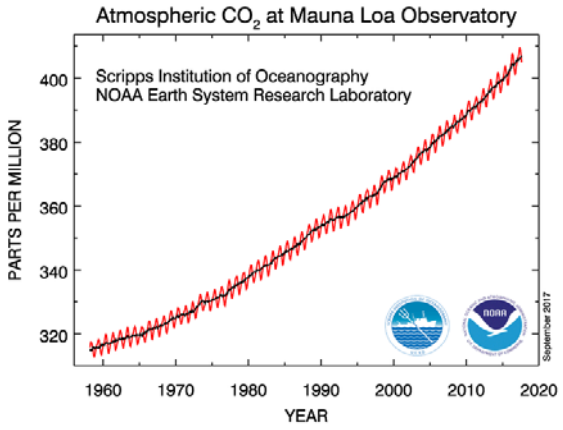

Figure 1: CO_2 concentration into the atmosphere along time [3].

A high concentration of CO_2 is directly related to global warming. In the 21st century, many countries are currently looking for ways of dealing with climate change concerns. In addition, alternative solutions to the use of fuels and other natural resources seem to be necessary.

Among the different available mitigation technologies able to reduce CO_2 emissions, Carbon Capture and Storage (CCS) technologies and Carbon Capture and Utilisation (CCU) approaches are particularly interesting. CCS represents the process of capturing CO_2 emissions in big amounts from large plants, such as fossil fuel power, transporting the captured CO_2 to safe geological storages. However, CCS development has many problems such as high costs investments, lack of positive public perception, environmental and safety concerns, and technological limitations [4, 5]. In this regard, alternative technologies to complement CCS are required [6]. CCU technology, like CCS, is based on the capture of CO_2 emissions in large amounts from large plants, even though the captured CO_2 is then converted into useful commercial products. Figure 2 shows a brief number of products that can be obtained from CO_2 and can be useful for industrial applications [7].

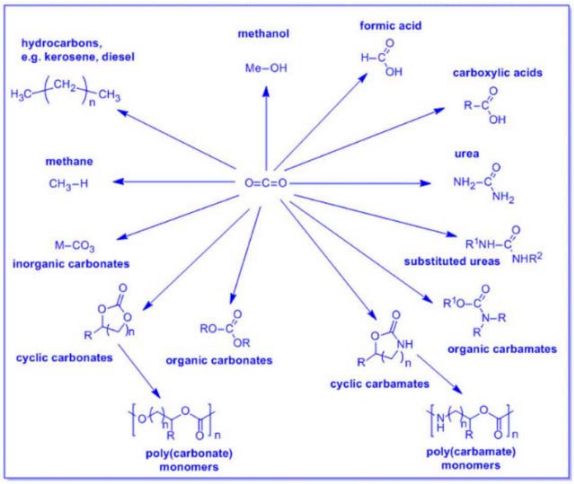

Figure 2: Different products from CO_2 reduction [7].

In addition, CCU avoids problems of costs and public acceptance which hinders CCS approaches. Moreover, CCU technologies allows us to storage intermittent renewable energies, such as wind and solar, in the form of chemical bonds, alleviating also our reliance on fossil fuels for chemical synthesis [8, 9].

There are several methods to activate and convert CO_2 such as chemical, thermochemical, photochemical, biochemical, electrochemical and hydrothermal [9]. Among them, the electrochemical approach is promising because of the possibility to carry out the CO_2 reduction at ambient conditions and the simple way to perform the process compared to other methods. In this regard, different reduction products can be obtained from CO_2 reduction, depending on the number of electrons and protons involved in the reaction [6, 10]:

(1) $CO_2 + 2H^+ + 2e^- \rightarrow CO + H_2O$

(2) $CO_2 + 2H^+ + 2e^- \rightarrow HCO_2H$

(3) $CO_2 + H^+ + 2e^- \rightarrow HCOO^-$

(4) $CO_2 + 4H^+ + 4e^- \rightarrow HCHO + H_2O$

(5) $CO_2 + 6H^+ + 6e^- \rightarrow CH_3OH + H_2O$

(6) $CO_2 + 8H^+ + 8e^- \rightarrow CH_4 + 2H_2O$

(7) $2CO_2 + 8H^+ + 8e^- \rightarrow HCOOCH_3 + 2H_2O$

(8) $2CO_2 + 10H^+ + 10e^- \rightarrow CH_3CHO + 3H_2O$

(9) $2CO_2 + 12H^+ + 12e^- \rightarrow C_2H_4 + 4H_2O$

(10) $2CO_2 + 12H^+ + 12e^- \rightarrow CH_3CH_2OH + 3H_2O$

(11) $3CO_2 + 14H^+ + 14e^- \rightarrow CH_3COOCH_3 + 4H_2O$

(12) $3CO_2 + 16H^+ + 16e^- \rightarrow CH_3COCH_3 + 5H_2O$

(13) $3CO_2 + 18H^+ + 18e^- \rightarrow CH_3CH(OH)CH_3 + 5H_2O$

(14) $3CO_2 + 18H^+ + 18e^- \rightarrow CH_3CH_2CH_2OH + 5H_2O$

The final product depends on the catalytic material used. For example, metals such as Au, Ag and Zn, are mainly leading to CO [11], Pb and Sn to obtain HCOOH [12], whereas Cu is able to electroreduce CO_2 to alcohols and hydrocarbons [12, 13]. Regarding the products obtained from CO_2, CH_3OH is one of the most interesting ones due to its stable storage properties and relatively high energy density. Additionally, it can be easily used in the current infrastructure for fuel transportation [14].

However, there are some issues that limit the practical application of this technology in the short-term. To begin with, CO_2 presents a high thermodynamic and kinetic stability and therefore, early activation is required for CO_2 reduction processes [15]. Since many products require a transfer of several electrons, kinetic reaction is slow, which can be enhanced by developing more active catalytic materials [8]. Moreover, mass transfer limitations in CO_2 reduction processes need to be tackled, because reaction rates are limited by the transfer of CO_2 from solution to the solid electrode surface [1, 11]. Gas diffusion electrodes (GDEs) have been proposed to alleviate mass transfer limitations [16-18]. GDEs allows to form a three-phase interface (gas-solid-liquid), which allows homogeneous distribution over the catalyst interface [2].

1.1 Catalytic materials

Different electrocatalytic materials have been investigated for the electrochemical reduction of CO_2, although their selectivity and efficiency need to be improved. On the other hand, the catalytic material stability should also be taken into account because most of the electrodes have shown remarkable decreases in selectivity and active abilities with time [2]. For example, as reported by Chang et al. [19], the formation of H_2 competed with CH_3OH formation at Cu_2O/ZnO-based electrodes, affecting the electrode

activity and stability, owing to the metal particles were separated from the electrode surface under continuous operation during hydrogen evolution reaction, and different defects on surface area might effect and to destabilise electrode surfaces, which may lead to the shortcoming of the electroreduction of CO_2 [20].

Different works have been reported in literature for the electrochemical reduction of CO_2 into CH_3OH using Mo, Ru and Cu as catalytic materials, including also their mixtures and oxidized forms in an attempt to make efficient and highly selective electrodes. In this regard, only Cu mixtures were found capable of producing CH_3OH with high reaction rates for sustainable periods of time [13, 21-23].

On the other hand, around thirty products have been obtained at Cu electrodes [24], including carbon monoxide (CO), formic acid (HCOOH), methane (CH_4), ethylene (C_2H_4) or ethane (C_2H_6), among others, although the current efficiencies and selectivities still need to be improved [25]. Thus, recent works have used a combination of Cu with other metals as electrocatalytic surfaces in order to improve reaction selectivities [13, 21-23, 26, 27].

The combination of two metals may improve electrode characteristics such as activity, stability and selectivity. In this sense, previous studies showed that mixture of materials might enhance the catalytic activity of electrodes [26-30]. For instance, the addition of Au into Cu-based electrodes showed a good catalytic activity for the formation of CH_3OH and C_2H_5OH in aqueous system [14] and the production of CO and H_2 [30]. Besides, the selectivity for CH_3OH and C_2H_5OH formation was improved using Cu/ZnO as catalytic material [27]. This fact might be explained because ZnO strength the Cu-C bond, which allows to improve the hydrogenation of the carbon atom.

In the last years, in an attempt to overcome catalytic material limitations, metal-organic frameworks (MOFs) seem to be promising [31, 32]. MOFs are hybrid materials, in which different electrocatalysts can be added according to the catalytic function required [9]. For instance, Kumar et al. [33] performed CO_2 reduction experiments at Cu-based MOF (HKUST-1) electrodes, highlighting the production of oxalic acid ($C_2H_2O_4$). In addition, Hinogami et al. [34] reported that Cu rubeanate MOF (CR-MOF)-based structures were useful for the production of HCOOH, Hod et al. [35] showed that iron–porphyrin-based MOFs exhibited high active-site exposure (10^{15} sites per cm^2) for the production of

syngas. Besides, Kornienko et al. [36] tested Co–porphyrin MOFs-based electrodes, showing a high stability (7 h) for syngas production.

To sum up, the combination of Cu with other metallic materials and the application of bimetallic MOFs seems to be very promising as electrocatalysts for CO_2 reduction, although a continuous development of these materials is required in order to enhance the performance of the process.

1.2 Electrochemical characterisation

The catalytic activity of the electrodes used in each case depends on interactions between catalytic sites and reactants [37]. In this sense, different techniques have been developed for characterising the materials. The main methods utilised in CO_2 reduction processes for electrochemically characterisation are cyclic voltammetry, CV (which defines the catalytic activity of the electrode materials) and Tafel plot, TP (which indicate step limitations of the reaction) [38].

CV is a type of potentiodynamic electrochemical measurement that can be used to analyse the catalytic activity of a material [39], in which kinetic and thermodynamic details can be evaluated [40]. Chemical reactions usually involve electron-transfer processes, whose finite rate depends on activation parameters such as the onset potential and the electrode activity [41].

The standard electrolysis cell consists of a working electrode, counter electrode, reference electrode, and electrolyte. Figure 3 shows an example of the experimental setup to perform a CV using a three-electrode cell [42].

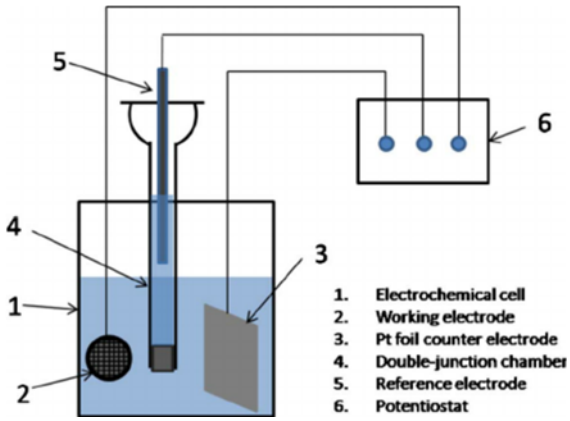

Figure 3: Example of a three electrode cell system [42].

Several authors have evaluated the influence of different electrocatalysts for the electrochemical reduction of CO_2 using CV. For instance, figure 4 shows the comparison between 5 types of Cu-based electrodes after 5 scans for alcohols formation from CO_2 electroreduction [9].

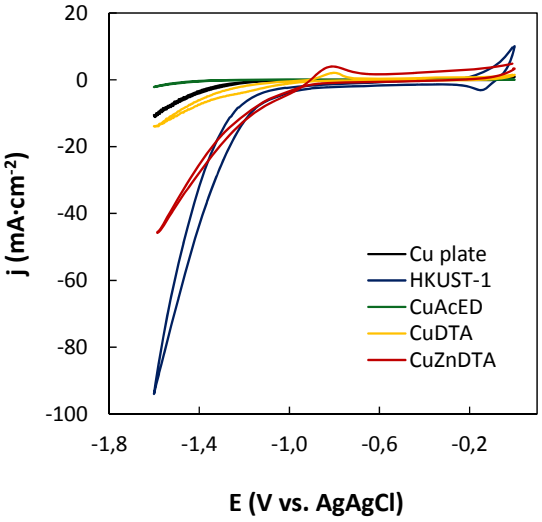

Figure 4: Cyclic voltammograms for the MOF-GDEs in a CO_2-saturated 0.5M $KHCO_3$ aqueous solution [9].

From the results, it can be observed that different catalytic responses were achieved as a function of the electrocatalytic material used [9].

On the other hand, another characterisation technique, namely TP can be useful to evaluate the limiting step of the process in a qualitative way [43].

TP is obtained from CV representations and it is based on the relation between the voltage and the logarithm of the generated current density at each potential level. As well as for the CV, TP could also be useful for comparison of different catalytic materials. For instance, figure 5 shows the TP for mesoporous carbon (MPC-1000) frameworks synthesized at 1000^{o}C as electrocatalysts for the reduction of CO_2 to CO [44].

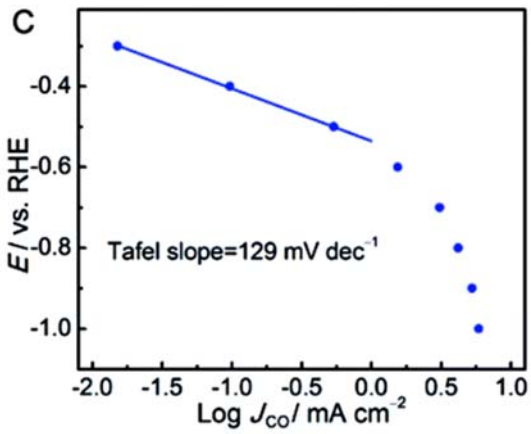

Figure 5: Tafel plot example under CO_2-saturated 0.1 M $KHCO_3$ conditions [44].

In this case, the reduction of CO_2 consists in two steps. Firstly, one electron is transferred to CO_2 to obtain $*CO_2^-$. Secondly, this $*CO_2^-$ is transferred and then converted into *CO, which was further reduced to CO.

1.3 Aim and objectives of the project

The aim of the present work is to perform the electrochemical characterization of bimetallic materials for CO_2 conversion. Accordingly, the objectives of the project are as follows:

- Preparation of the catalytic inks (bimetallic and bimetallic MOF-based materials)
- Preparation of the cathode materials
- Cyclic voltammetry measurements. Influence of catalytic loading, presence/absence of CO_2 and material stability
- Tafel plot analyses
- Comparison of results

2 Methodology and Materials

2.1 Materials

1. Carbon Black Powder (VXC72R, CABOT).
2. PTFE preparation 60 wt% (Sigma-Aldrich) (polytetrafluoroethylene).
3. Nafion dispersion 5 wt% in water (Alfa Aesar).
4. $KHCO_3$ (PanReac).
5. Isopropanol (Sigma-Aldrich).
6. HKust-1 (Cu).
7. HPd10 (Cu 90 wt%, Pd 10 wt%).
8. HZn10 (Cu 90 wt%, Zn 10 wt%).
9. HRu10 (Cu 90 wt%, Ru 10 wt%).
10. HBi5 (Cu 95 wt%, Bi 5 wt%).
11. HBi20 (Cu 80 wt%, Bi 20 wt%).
12. CAU-17 (Bi 100%).
13. HBi10 (mix) (HKust 90 wt%, CAU17 10 wt%).
14. Cu (copper).
15. Cu-Au (Cu 99 wt%, Au 1 wt%).
16. Cu-Mo (Cu 99 wt%, Mo 1 wt%).
17. Cu-Ru (Cu 99% wt., Ru 1 wt%).
18. Cu-Pd (Cu 99% wt., Pd 1 wt%).
19. UP (ultra-pure water).

The next electrodes were prepared as a function of the catalytic loading:

a) 0.5 mg/cm^2: Cu, Cu-Mo and Cu-Pd.

b) 1 mg/cm^2: Cu, Cu-Mo, Cu-Ru, Cu-Pd, Cu-Au, HKUST-1, HPd10, HZn10, HRu10, HBi5, HBi20, HBi10 (mix) and CAU-17.

c) 2 mg/cm^2: Cu, Cu-Mo and Cu-Pd.

Notation: HKUST-1 is MOF with Cu in his structure; the initial H involves the presence of HKUST-1; CAU-17 is MOF with only Bi in the structure; HBi10 (mix) – physical mixture of HKUST-1 and CAU-17; the number at the end represents the percentage of the second metal. For example HPd10 consist of 90 wt% Cu and 10 wt% Pd.

2.2 Inks preparation

The microporous layer inks were formed by a mixture of Carbon Black Powder particles (VXC72R, CABOT) and PTFE (Polytetrafluoroethylene, Sigma-Aldrich, 60 wt% dispersion in H_2O) with a 70:30 Vulcan/PTFE mass ratio. This mixture was then diluted to 3 % in isopropanol (IPA) (99.5%, Sigma-Aldrich). The final mixtures were sonicated for 30 min in an ultrasound bath. On the other hand, the catalytic inks were prepared by mixing bimetallic particles as electrocatalysts, a Nafion solution (5 wt% Alfa Aesar) as binder and IPA (99.5%, Sigma-Aldrich) as vehicle, with a 70/30 (electrocatalyst/Nafion) mass ratio and a 3% solids (electrocatalyst + Nafion). The obtained mixtures were also sonicated for 30 min.

2.3 Electrode preparation

The Micro-porous layer (MPL) were prepared by air-brushing a Vulcan carbon powder-based ink onto a porous carbon paper support (TGP-H60, Toray Inc.). MPLs were obtained with a carbon powder loading of 2.6 mg/cm^2 by accumulation of layers and complete IPA evaporation during the airbrushing step. The final step consisted of inserting the MPLs-based electrodes into a muffle furnace (Mod. 12 PR/300 SERIE 8B, Hobersal) at 350^{o}C for 30 minutes to induce sintering of the carbon black particles. Figure 6 shows a picture of the air-brushed MPL.

Figure 6: Prepared MPL.

Cu-based electrodes (99 wt% Cu and 1 wt% other material) with a geometric area, A= 10 cm^2 were obtained by air-brushing a catalytic ink onto a porous carbon paper with a MPL layer. The Cu-based electrodes with different catalytic loadings were also prepared by simple accumulation of layers and complete IPA evaporation during the air-brushing process. This last fact was verified by weighing the electrode. The same procedure was carried out to obtain the MOF-based electrodes.

2.4 Cyclic Voltammetry tests

The electrochemical activity of the electrodes was evaluated by CVs at a scan rate of 50 mV/s. A 0.1 M $KHCO_3$ aqueous solution (under CO_2 or N_2 conditions) was used as electrolyte in a standard three-electrode undivided electrochemical cell equipped with a graphite rod as the counter electrode and an Ag/AgCl (sat. KCl) as the reference electrode, as shown in figure 7. Small portions (about 1.5 cm^2 area) of the prepared electrodes were cut and used as working electrodes. An AutoLab PGSTAT 302N potentiostat (MSTAT4, Arbin Instruments) was used to carry out the CV tests. The applied potential ranged from 0 V to −2 V vs. Ag/AgCl and the samples were five times cycled. In addition, one of the MOF-based samples was 40 times cycled in order to analyse the stability of the material. The presence/absence of CO_2 into the electrolyte was also tested.

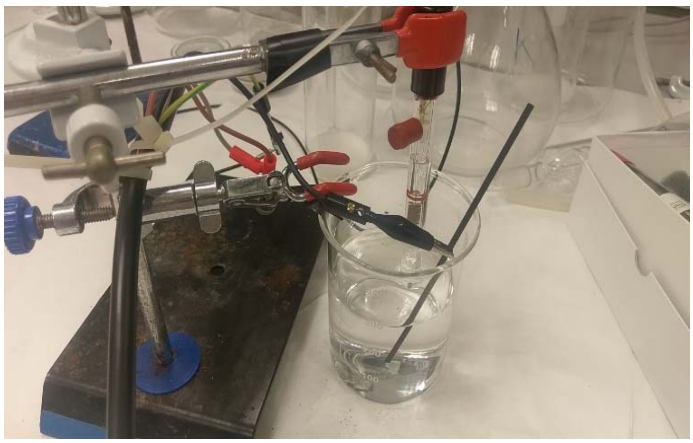

Figure 7: Cyclic Voltammetry system.

3 Results and discussion

3.1 Cyclic voltammetry

3.1.1 Cu electrode

Figure 8 shows the CV responses for the carbon paper, MPL (2.6 mg/cm^2) and Cu (1 mg/cm^2) under CO_2 conditions.

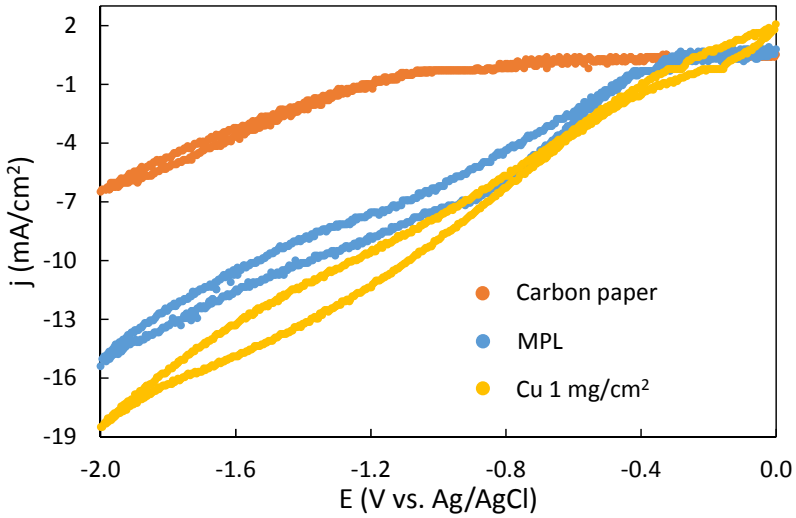

Figure 8: Catalytic activity comparison between carbon paper, MPL and Cu.

The lowest catalytic activity (-6.38 mA/cm^2) was achieved at the carbon paper-based electrode due to the fact that no catalytic surface is present on it. The addition of the MPL increases the electrode conductivity, involving a higher activity (-15.39 mA/cm^2) than carbon paper. In addition, MPL may alleviate mass transfer limitation in the CO_2 electroreduction process. As expected, the presence of the catalytic material (Cu) within the electrode involves the highest catalytic activity.

In an attempt to evaluate the influence of the catalytic loading, figure 9 shows the cyclic voltammetry responses for the Cu electrodes at different catalytic loadings (0.5, 1 and 2 mg/cm^2) in a 0.1 M $KHCO_3$ aqueous CO_2 saturated solution after 5 scans. Figure 10 represents a zoom of figure 9.

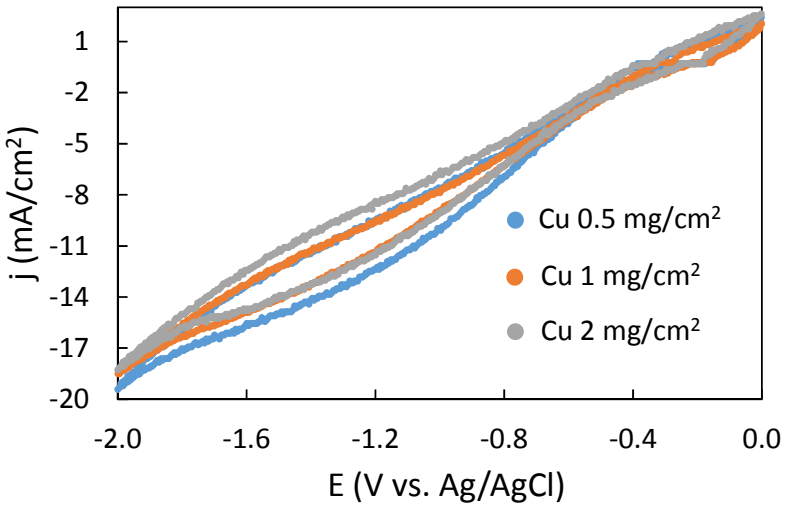

Figure 9: CVs for Cu electrodes with different catalytic loadings under CO_2 conditions.

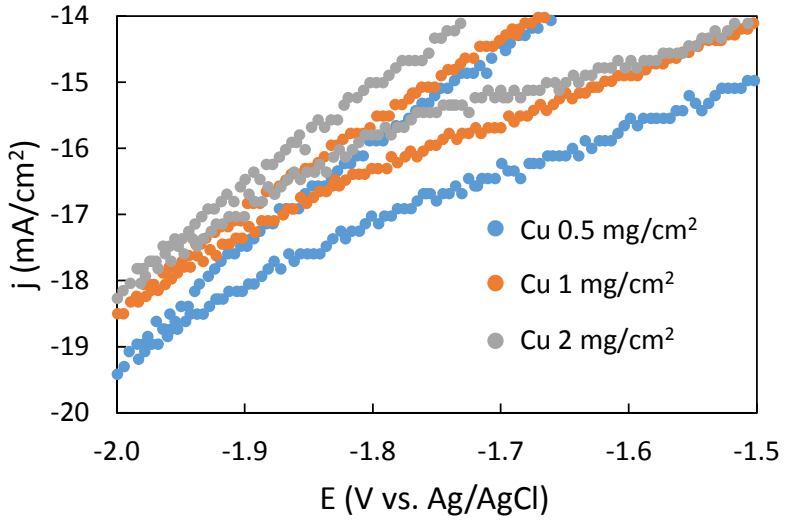

Figure 10: Zoom of figure 9 between -14 and -20 mA/cm^2.

The highest catalytic activity (-19.4 mA/cm^2) was achieved at 0.5 mg/cm^2, whereas the lowest response was obtained at 2 mg/cm^2 (-18.2 mA/cm^2), although similar values are observed in all cases. The slight differences may be related to particle agglomeration at higher catalytic loadings, involving a decrease in the final activity.

In an attempt to evaluate the effect of the presence of CO_2, cyclic voltammetry experiments were performed under N_2 saturation. The electrolyte was bubbled with N_2 for 25 minutes. Figure 11 shows cyclic voltammetry results obtained for Cu (1 mg/cm^2) electrode with presence /absence CO_2 and figure 12 represents a zoom of figure 11.

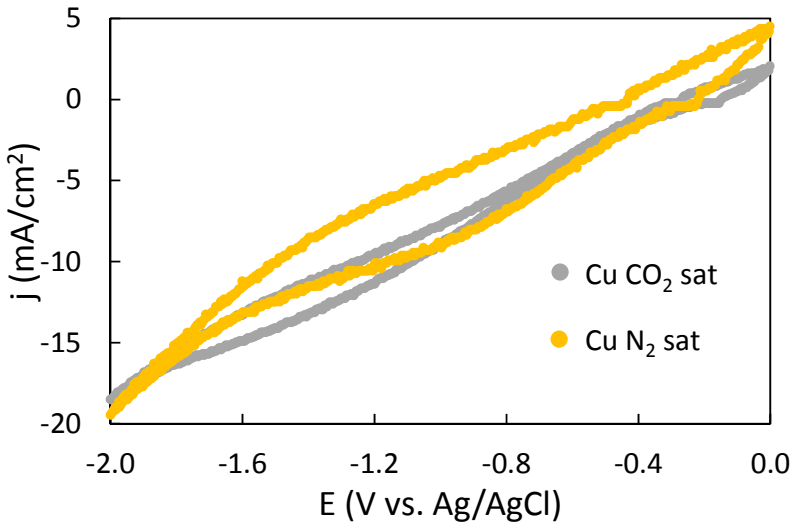

Figure 11: CVs for the Cu electrode (1 mg/cm^2) under CO_2 and N_2 conditions.

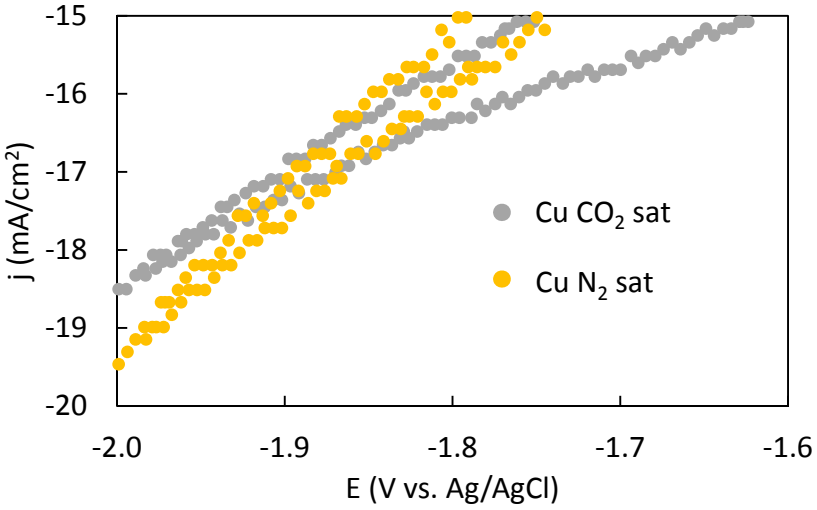

Figure 12: Zoom for figure 11 between -15 and -20 mA/cm^2.

No significant differences can be observed in terms of catalytic activity (-18.50 mA/cm^2 for CO_2 sat. and -19.46 mA/cm^2 for N_2 sat.), which may be explained by the effect of the hydrogen evolution reaction.

3.1.2 Cu-based bimetallic materials

Figure 13 shows the CVs for the bimetallic electrodes containing Cu in combination with other metals (Au, Ru, Pd and Mo), in comparison to the Cu electrode under CO_2 conditions. These second metals were selected because of their possible ability to enhance the adsorption of intermediate species and reduce the overpotential of the

reaction [12]. For instance, the addition of Au have been previously reported for the formation of CO [6] and alcohols [26] under different conditions.

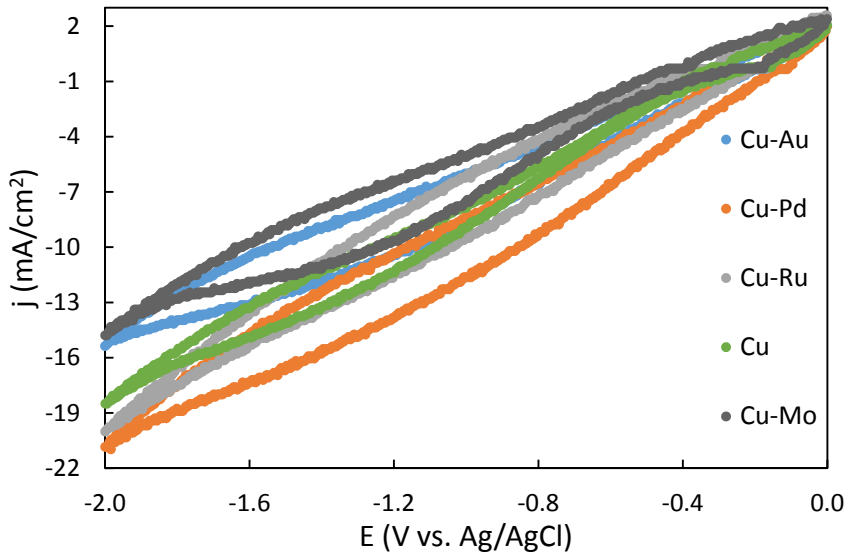

Figure 13: CVs for bimetallic materials (Au, Ru, Pd and Mo) under CO_2 conditions.

Cu-Pd (-20.85 mA/cm^2) and Cu-Ru (-20.01 mA/cm^2) electrodes reached the highest catalytic activities, whereas the lowest activities was achieved by the electrodes made of Cu-Au (-15.37 mA/cm^2) and Cu-Mo (-14.79 mA/cm^2). In any case, Cu-Pd and Cu-Ru seems to be the best candidates for the electroreduction of CO_2 in terms of current-voltage response.

This high activity achieved at Cu-Pd based electrodes might be related to a better adsorption of intermediate products on electrode surface, involving a modification in reaction mechanisms [24, 45].

Figures 14 and 15 show the CV responses for Cu-Mo and Cu-Pd electrodes, respectively, in the presence of CO_2 after 5 scans at three different catalytic loadings (ranging from 0.5 mg/cm^2 to 2 mg/cm^2).

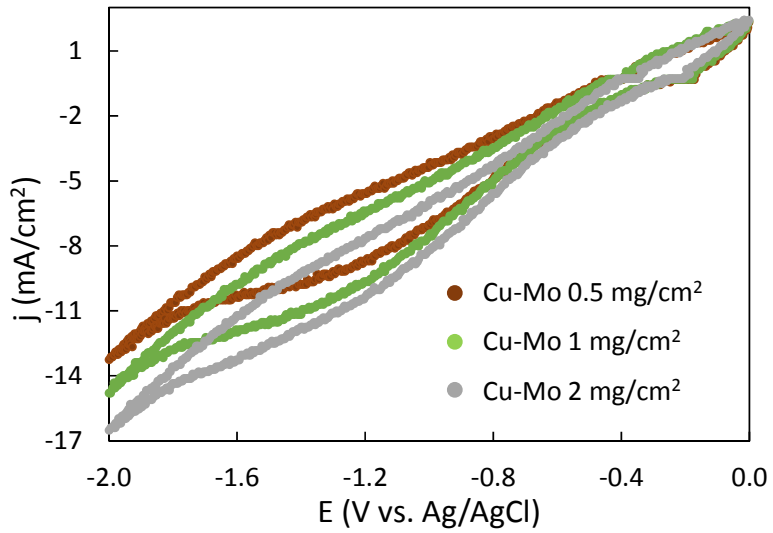

Figure 14: CVs for Cu-Mo electrodes with different catalytic loadings in the presence of CO_2.

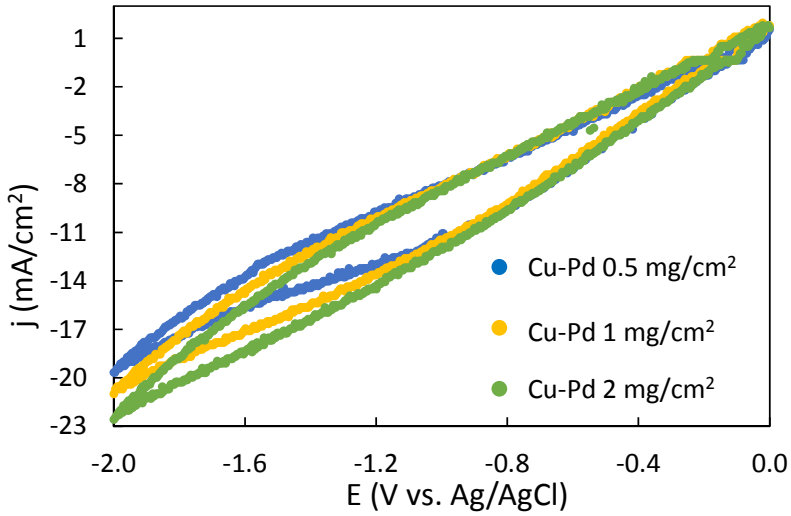

Figure 15: CVs for Cu-Pd electrodes with different catalytic loadings in the presence of CO_2.

Regarding the Cu-Mo-based electrodes, an increase in the catalytic loading involved higher activities (-16.5 mA/cm² at 2 mg/cm²). Conversely, no clear differences were observed at Cu-Pd materials. Comparing the CV responses, a higher catalytic activity was achieved for the Cu-Pd-based electrodes in the whole catalytic loading range studied, which might be associated with differences in reaction mechanisms and product distribution.

Overall, there are no very significant differences at Cu-Pd-based electrodes in terms of the reached current density at -2 V vs. Ag/AgCl, even though Cu electrodes showed particle agglomeration at higher catalytic loadings, whereas Cu-Mo-based electrodes presented a slightly higher response when increasing the catalytic loading. In this regard,

the effect of the presence/ absence of CO_2 is evaluated at a catalytic loading of 1 mg/cm^2.

CV profiles under CO_2 and N_2 conditions for Cu-Pd, Cu-Au and Cu are represented from figure 16 to figure 18.

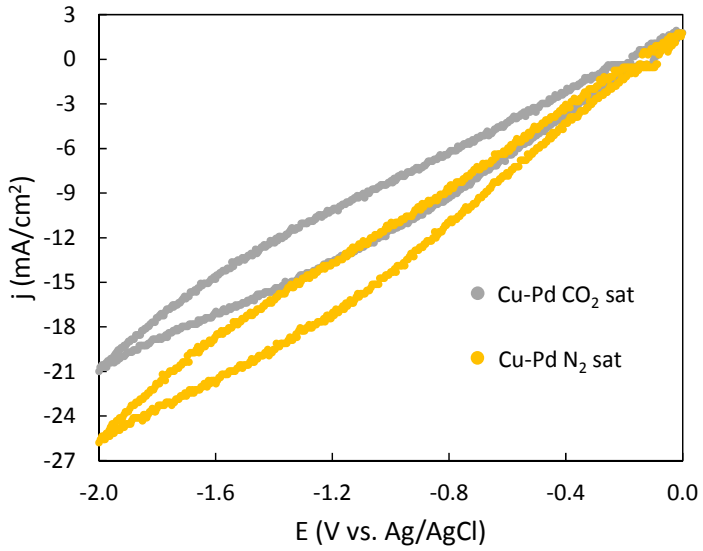

Figure 16: CVs for Cu-Pd electrode (1 mg/cm^2) under CO_2 and N_2 conditions.

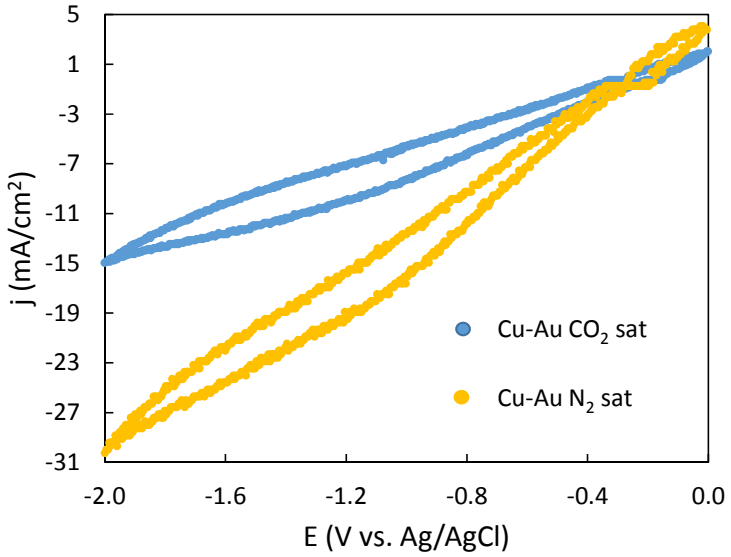

Figure 17: CVs for Cu-Au electrode (1 mg/cm^2) under CO_2 and N_2 conditions.

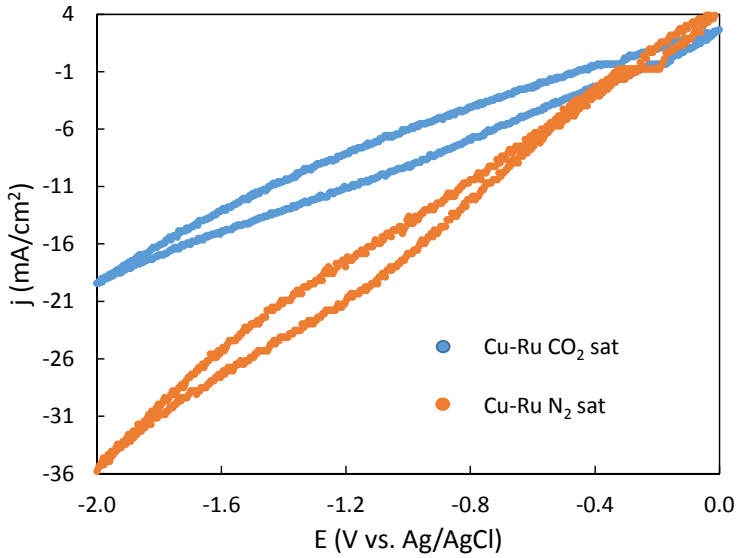

Figure 18: CVs for Cu-Ru electrode (1 mg/cm^2) under CO_2 and N_2 conditions.

Similar trends can be observed in the three figures. A higher catalytic activity has been reached under N_2 conditions owing to the effect of the hydrogen evolution at these Cu-based materials that competes with CO_2 reduction in case of saturation with this gas, involving lower responses.

The highest activity (N_2-saturated solution) was achieved using Cu-Ru-based surfaces (-36 mA/cm^2), whereas lower activities (-30 mA/cm^2 and -26 mA/cm^2) were reached at Cu-Au and Cu-Pd electrodes, respectively. However, under CO_2 conditions, Cu-Pd electrodes showed the highest activity (-21 mA/cm^2) in comparison with Cu-Ru (-20 mA/cm^2) and Cu-Au (-15 mA/cm^2)-based surfaces.

3.1.3 MOFs

Figure 19 shows the CV results obtained for MOFs-based electrodes at 1 mg/cm^2 in the presence of CO_2. The CV response for Cu has been also included for comparison. It is important to note that most MOFs tested in this work are also bimetallic materials, unlike the HKUST-1 (100% Cu) and the CAU-17 (100% Bi), which have also been included for comparison.

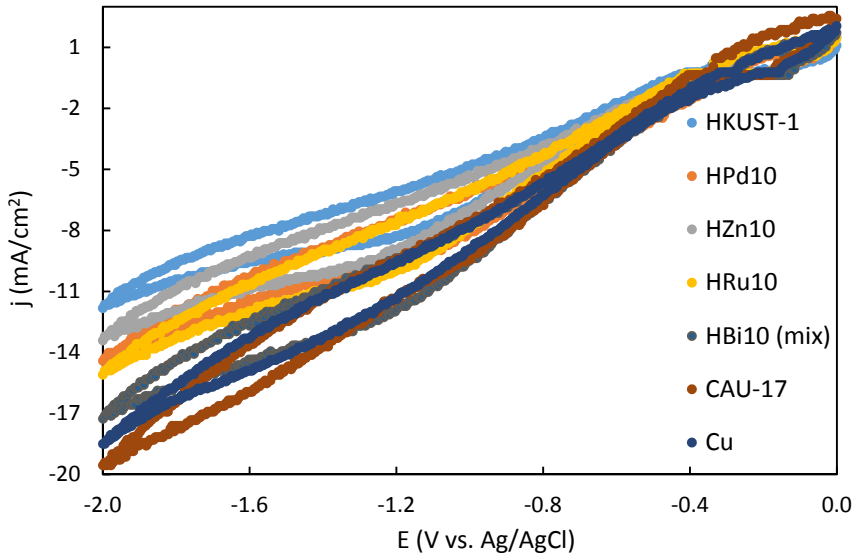

Figure 19: CVs for MOFs materials with 1 mg/cm^2 under CO_2 conditions.

Most MOF-based materials showed a lower activity than the obtained for the Cu electrode. However, CAU-17-based electrode, which is composed entirely of Bi, reached the highest current-voltage response at -2 V vs. Ag/AgCl (-19.55 mA/cm^2).

Additionally, Figure 20 shows the CV responses in the presence of CO_2 for three MOFs that contain different amounts of Bi in combination with Cu (HBi5, HBi10mix and Hbi20) in order to evaluate the effect of the weight percent of Bi. For the sake of clarity, Figure 21 shows a zoom of figure 20 between -12 mA/cm^2 and -18 mA/cm^2.

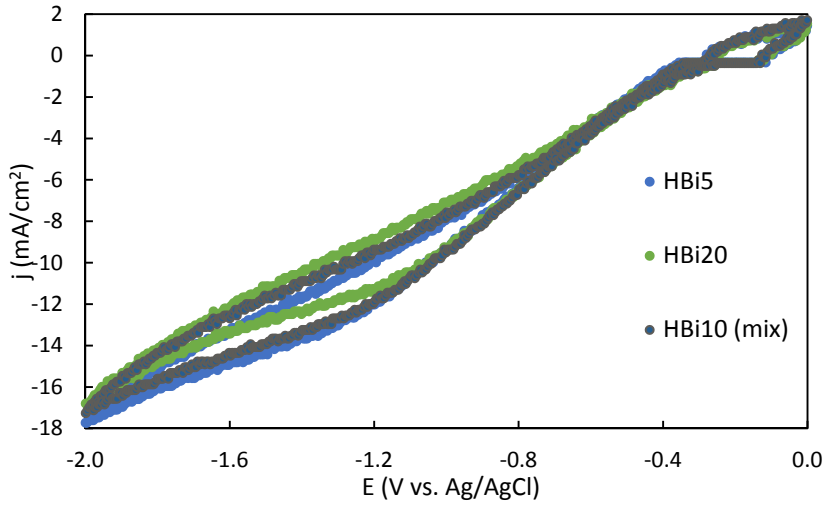

Figure 20: Effect of adding Bi in Cu-based MOF structure in the presence of CO_2.

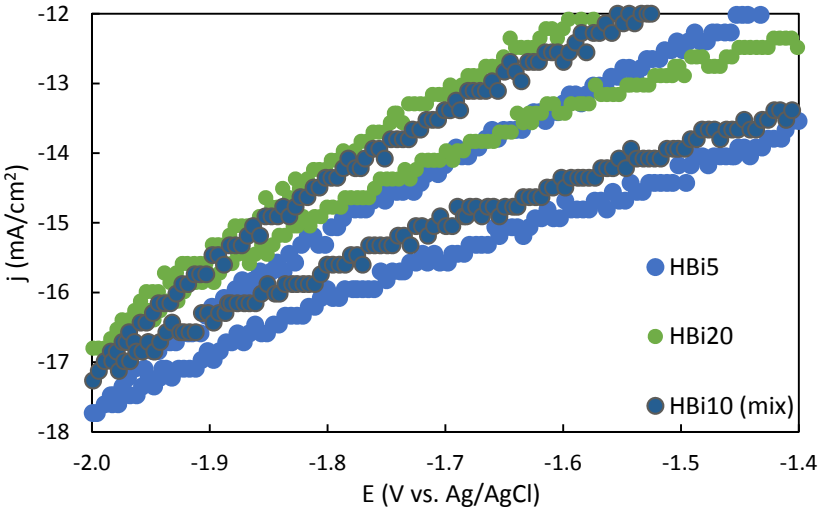

Figure 21: Zoom for figure 20 between -12 and - 18 mA/cm^2.

The effect of adding different amounts of Bi in the MOF structure showed slight differences in the final activity of the electrodes (-17.7 mA/cm^2 against -16.8 mA/cm^2 for HBi5 and HBi20, respectively).

In this regard, the effect of the presence/ absence of CO_2 has been evaluated in figure 22 for the most active material (i.e. HBi5) at -2 V vs. Ag/AgCl.

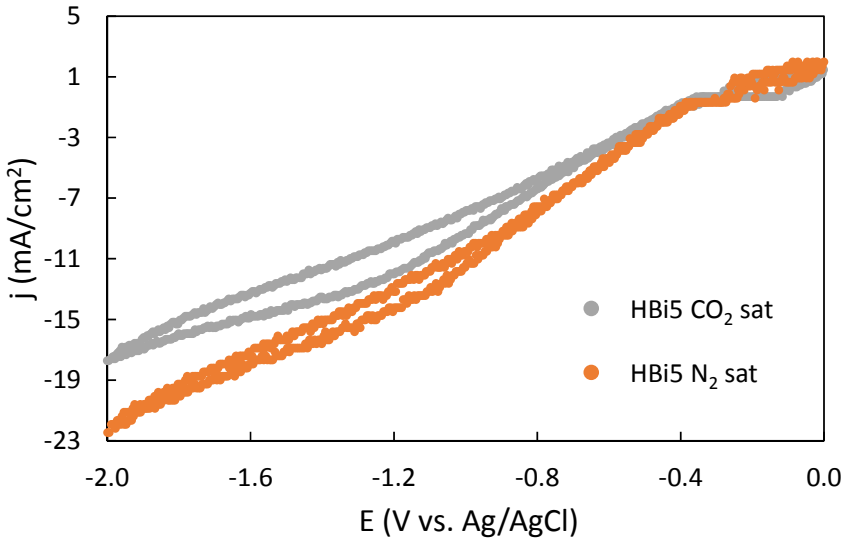

Figure 22: CVs for HBi5 electrode (1 mg/cm^2) under CO_2 and N_2 conditions.

The highest activity was reached for the N_2-saturated electrolyte (-22.5 mA/cm^2) compared to those obtained under CO_2 conditions (-17.6 mA/cm^2) because the formation of H_2 competes with the CO_2 reduction reaction.

Moreover, the evaluation of the stability of the electrodes is crucial for further applications in CO_2 reduction processes. In this sense, Figure 23 represents the CV

stability tests (material cycled 40 times) for HBi5-MOF at 1 mg/cm^2. Figure 24 has been also included for the sake of clarity.

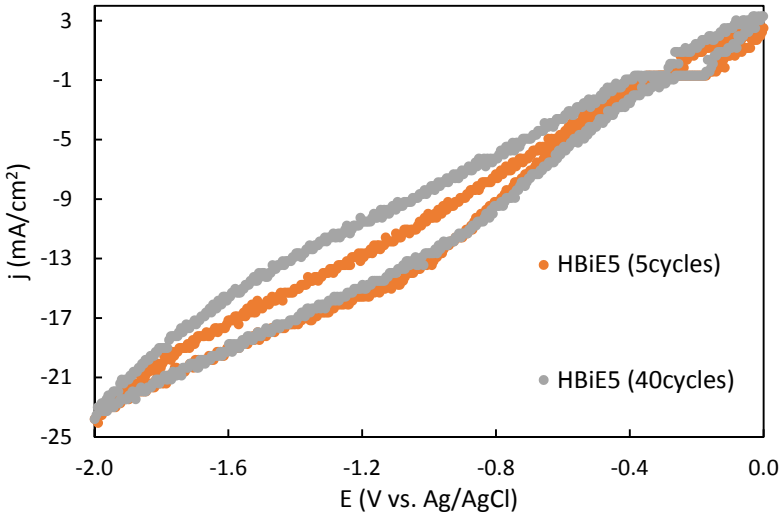

Figure 23: Stability test for HBi5 electrode (1 mg/cm^2) under CO_2 conditions.

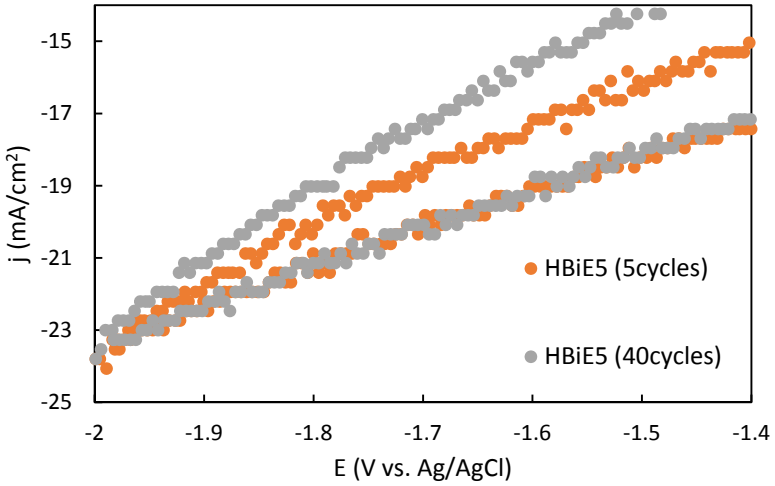

Figure 24: Zoom of figure 23 between -14 and -25 mA/cm^2.

Previous MOFs studies showed a decrease in their catalytic activity for a long period of time because of their limited stability in water [46, 47]. However, HBi5-MOF showed a significance stability after 40 cycles, which is particularly interesting from an applicability point of view in terms CO_2 reduction reaction in liquid media. Further works should include stability test for a much longer period of time to identify possible deactivation of the catalytic material.

3.1.4 Comparison of the most active materials (bimetallics and MOFs)

To summarise, Figure 25 shows the current-voltage responses of the most active MOF that contains Cu (HBi5), the Cu electrode and the most active bimetallic-based electrode (Cu-Pd) in a CO_2-saturated electrolyte.

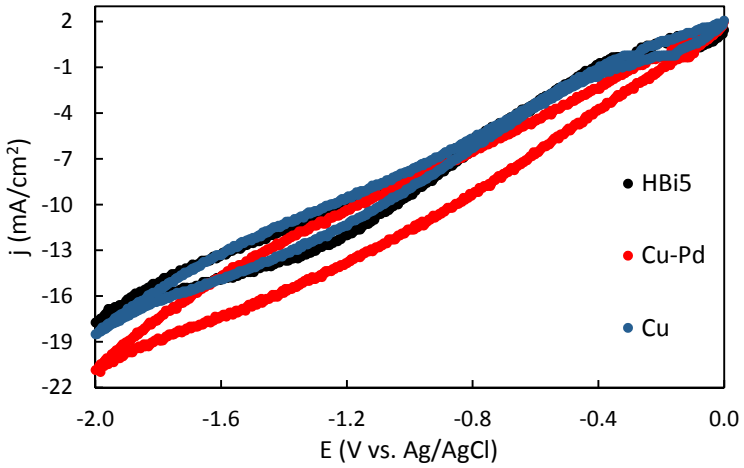

Figure 25: Comparison of Cu, Cu-Pd and HBi5 under CO_2 conditions.

The comparison shows that Cu-Pd seems to be the most active material in terms of current-voltage response, even though all the prepared materials need to be tested using an electrochemical cell in order to analyse the selectivity, productivity and efficiency for CO_2 reduction to different products.

3.2 Tafel plots

As discussed above, the step limitations of CO_2 electroreduction processes can be studied using TP analyses by evaluating the resulting slopes in each case. Regarding the literature, the first slope represents the activation of CO_2 (to form $CO_2^{\cdot-}$) at low negative potentials. In this regard, this work focuses on this slope because the product distribution from CO_2 reduction has not been evaluated. As a result, the reduced products in each case cannot be identified. According to Tafel equation for electrokinetic reaction, lower the value of the Tafel slope corresponds to fast kinetics for this step [48-55]. Figure 26 shows the results for the Cu electrode, the most active bimetallic material (Cu-Pd) and the most active bimetallic MOF-based material that contains Cu (HBi5).

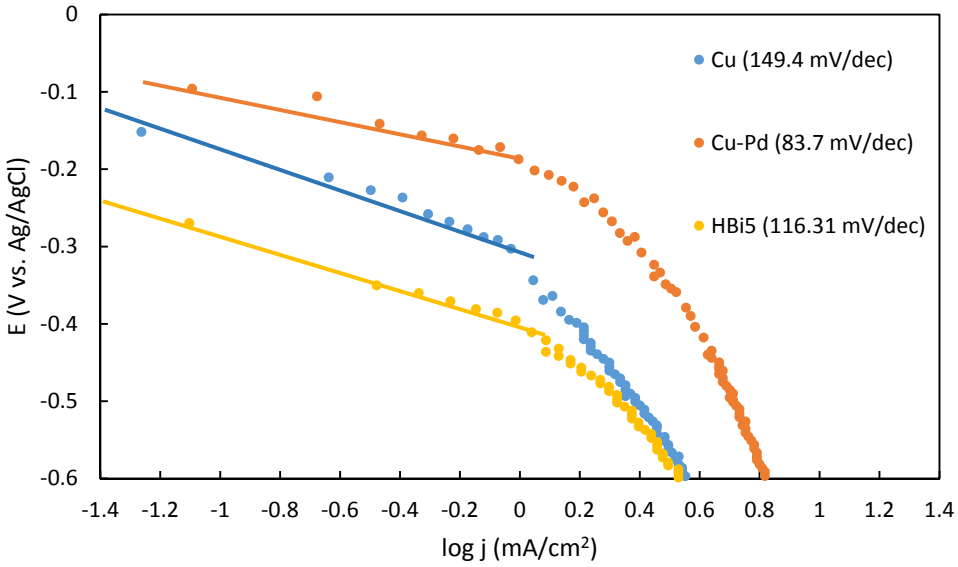

Figure 26: Tafel plot for Cu, Cu-Pd and HBi5-based electrodes.

Slight differences between Tafel slopes for Cu, Cu-Pd and HBi5-based electrodes can be observed. The lowest slope corresponds to the Cu-Pd electrode (83.7 mV/dec), whereas the highest value was obtained for the Cu electrode (149.4 mV/dec). As a consequence, Cu-Pd electrodes would involve a lower kinetic barrier, which means that the energy requirements for the activation of CO_2 will be lower. In contrast, the use of Cu electrodes for CO_2 electroreduction might involve higher energy requirements and kinetic barriers to carry out the reduction of CO_2 into $CO_2^{\cdot-}$. To sum up, the TPs showed that the combination of Cu and Pd and the application of a bimetallic MOF structure (HBi5) would require less energy for the activation of CO_2 compared to the Cu electrode.

4 Conclusions

In this work, the electrochemical activity of bimetallic materials (i.e. Cu-Au, Cu-Mo, Cu-Ru and Cu-Pd) and bimetallic metal-organic frameworks (i.e. HKUST-1, HPd10, HZn10, HRu10, HBi5, HBi20, HBi10mix and CAU-17) is evaluated. The electrodes were prepared by air-brushing a microporous layer into a carbon paper support. The catalytic layers were then air-brushed onto it using different catalytic loadings (ranging from 0.5 mg/cm^2 to 2 mg/cm^2). The materials were electrochemically characterised by cyclic voltammetric analyses using a standard three electrode electrochemical cell (0.1 M $KHCO_3$ as electrolyte) at a potential range between 0 V to −2 V vs. Ag/AgCl (5 cycles). The most active materials were further characterised by Tafel plot analyses.

The most active bimetallic material in terms of current-voltage response was Cu-Pd (-20.98 mA/cm^2), whereas the lowest activity was reached for the Cu-Mo electrode (-14.79 mA/cm^2) in a CO_2-saturated electrolyte. In this case, an increase in the catalytic loading of bimetallic materials involves not very significant differences in terms of current-voltage responses. In addition, all the bimetallic materials presented higher activities under N_2 conditions, which might be associated with the effect of the hydrogen evolution reaction, competing with CO_2 conversion in the presence of CO_2.

Among the bimetallic metal organic framework materials tested, HBi5 showed the highest catalytic activity (-17.73 mA/cm^2) under CO_2 conditions. In addition, the stability test for this material showed an interesting stable performance along time (40 cycles).

To sum up, the most active bimetallic and metal organic framework materials were compared with Cu electrodes. In general, bimetallic electrodes showed higher activities than the bimetallic metal organic framework-based electrodes tested. Finally, Tafel plot analyses showed that Cu-Pd presented the fastest kinetics for the activation of CO_2 compared to those obtained for HBi5 and Cu electrodes. Thus, Cu-Pd-based electrodes seem to be interesting for CO_2 electroreduction processes, even though further electrochemical cell tests are needed to analyse the selectivity, productivity and efficiency of these materials for CO_2 electroreduction.

References

1. Albo J., Saez A., Jose S.G., Vicente M., Irabien A., Appl. Catal. B., 2015, 176‑177, 709‑717.
2. Albo J., Irabien A., Journal of Catalysis, 2016, 343, 232–239.
3. Mauna Loa Observatory, National Oceanic & Atmospheric Administration, 2017, 30/09/17, www.esrl.noaa.gov/gmd/ccgg/trends/full.html
4. Meylan F.D., Moreau V., Erkman S., J. CO_2 Util., 2015, 12, 101-108.
5. Gibbins J., Chalmers H., Energy Policy, 2008, 36, 4317-4322.
6. Merino-Garcia I., Alvarez-Guerra E., Albo J., Irabien A., Chem. Eng. J., 2016, 305, 104-120.
7. Styring P., Jansen D., de Coninck H., Reith H., Armstrong K., Centre for Low Carbon Futures ,2011, 14/08/17, http://co2chem.co.uk/wp-content/uploads/2012/06/CCU%20in%20the%20green%20economy%20report.pdf
8. Jhong H.R.M., Ma S., Kenis P.J.A., Curr. Opin. Chem. Eng., 2013, 2, 191-199.
9. Albo J., Vallejo D., Beobide G., Castillo O., Castano P., Irabien A., ChemSusChem, 2016, 9, 1–11.
10. Gutiérrez-Guerra N., Moreno-López L., Serrano-Ruiz J. C., Valverde J. L., Appl. Catal. B., 2016, 188, 272-282.
11. Alvarez-Guerra M., Quintanilla S., Irabien A., Chem. Eng. J., 2012, 207, 278-284.
12. Qiao J., Liu Y., Hong F., Zhang J., Chem. Soc. Rev., 2014, 43, 631-675.
13. Peterson A.A., Abild-Pedersen F., Studt F., Rossmeisl J., Norskov J.K., Energy Environ. Sci., 2010, 3, 1311-1315.
14. Albo J., Alvarez-Guerra M., Castano P., Irabien A., Green Chem.,2015, 17, 2304-2324.
15. Oana R. Luca, Charles C. L. McCrory, Nathan F. Dalleska, Carl A. Koval, J. Electrochem. Soc., 2015, 162, H473-H476.
16. Del Castillo A., Alvarez-Guerra M., Irabien A., AIChE J., 2014, 60 (10), 3557-3564.
17. Wang Q., Dong H., Yu H., RSC Adv., 2014, 4, 59970-59976.
18. Wang Q., Dong H., Yu H., J. Power Sources, 2014, 271, 278-284.
19. Chang T.Y., Liang R.M., Wu P.W., Chen J.Y., Hsieh Y.C., Mat. Lett., 2009, 63, 1001–1003.
20. Frese K.W., J. Electrochem. Soc., 1991, 138 (11), 3338–3344.
21. Hori Y., Kikuchi K., Suzuki S., Chem. Lett., 1985, 14, 1695-1698.
22. Hori Y., Kikuchi K., Murata A., Suzuki S., Chem. Lett., 1986, 15, 897-898.
23. Gattrell M., Gupta N., Co A., J. Electroanal. Chem., 2006, 594, 1-19.
24. Kuhl K. P., Cave E. R., Abram D. N., Jaramillo T. F., Energy Environ. Sci., 2012, 5, 7050–7059.
25. Appel A. M., Bercaw J. E., A. B. Bocarsly, Dobbek H., DuBois D. L., Dupuis M., Ferry J. G., Fujita E., Hille R., Kenis P. J., Chem. Rev., 2013, 113, 6621–6658.
26. Jia F., Yu X., Zhang L., J. Power Sources, 2014, 252, 85–89.
27. Andrews E., Ren M., Wang F., Zhang Z., Sprunger P., Kurtz R., Flake J., J. Electrochem. Soc., 2013, 160 (11), H841–H846.
28. Lan Y., Ma S., Lu J., Kenis P.J.A., Int. J. Electrochem. Sci., 2014, 9, 7300–7308.
29. Rasul S., Anjum D. H., Jedidi A., Minenkov Y., Cavallo L., Takanabe K., Angew. Chem. Int. Ed., 2015, 54, 2146-2150.
30. Zhu S., Shao M., J. Solid State Electrochem., 2016, 20, 861-873.
31. Gascon J., Corma A., Kapteijn F., Llabres I Xamena F. X., ACS Catal., 2014, 4, 361–378.
32. Liu Y., Wang Z. U., Zhou H. C., Greenhouse Gases Sci. Technol., 2012, 2, 239–259.

33. Kumar R. S., Kumar S. S., Kulandainathan M. A., Electrochem. Commun., 2012, 25, 70–73.
34. Hinogami R., Yotsuhashi S., Deguchi M., Zenitani Y., Hashiba H., Yamada Y., ECS Electrochem. Lett., 2012, 1, H17–H19.
35. Hod I., Sampson M. D., Deria P., Kubiak C. P., Farha O. K., Hupp J. T., ACS Catal., 2015, 5, 6302–6309.
36. Kornienko N., Zhao Y., Kley C. S., Zhu C., Kim D., Lin S., Chang C. J., Yaghi O. M., Yang P., J. Am. Chem. Soc., 2015, 137, 14129–14135.
37. Haensel V., Hansel H. S., American Chemical Society: Washington, DC, 1989, DOI: 10.1021/bk-1989-0411.ch001.
38. Gutman E.M., Corrosion Science, 2005, 47, 3086-3096.
39. University of Cambridge, Department of Chemical Engineering and Biotechnology, 11/09/2017.
https://www.ceb.cam.ac.uk/research/groups/rg-eme/teaching-notes/linear-sweep-and-cyclic-voltametry-the-principles.
40. Scholz F. (ed), Electroanalytical Methods, 2nd ed., 2010, 57-102.
41. Heinze J., Angew. Chem. Int. Ed. Engl., 1984, 23, 831-847.
42. Liu Z. Y., Zhang J. L., Yu P. T., Zhang J. X., Makharia R., More K. L., Stach E. A., J. Electrochem. Soc., 2010, 157, B906-B913.
43. University of Cambridge, Department of Chemical Engineering and Biotechnology, 20/09/17,
https://www.doitpoms.ac.uk/tlplib/aqueous_corrosion/tafel_plot.php.
44. Pan F., Liang A., Duan Y., Liu Q., Zhang J., Li Y., J. Mater. Chem. A., 2017, DOI: 10.1039/C7TA03005C.
45. Ohkawa K., Hashimoto K., Fujishima A., Noguchi Y., Nakayama S., J. Electroanal. Chem., 1993, 345, 445–456.
46. Huang L. M., Wang H. T., Chen J. X., Wang Z. B., Sun J. Y., Zhao D. Y., Yan Y. S., Microporous Mesoporous Mater., 2003, 58, 105–114.
47. Hausdorf S., Wagler J., Mossig R., Mertens F. O., J. Phys. Chem. A., 2008, 112, 7567–7576.
48. Zhang H., Nai J., Yu L., Lou X.W., Joule, 2017, 1, 77-107.
49. Zhang H., Ma Z., Liu G., Shi L., Tang J., Pang H., Wu K., Takei T., Zhang J., Yamauchi Y.,Ye J., NPG Asia Materials, 2016, doi:10.1038/am.2016.102.
50. Guan B. Y., Yu L., Lou X. W., Angew. Chem. Int. Ed., 2017, 56, 2386-2389.
51. Xiao X., He C. T., Zhao S., Li J., Lin W., Yuan Z., Zhang Q., Wang S., Dai L., Yu D., Energy Environ. Sci., 2017, 10, 893-899.
52. Jiang N., You B., Sheng M., Sun Y., Angew. Chem. Int. Ed., 2015, 54, 6251-6254.
53. Wu J., Yadav R. M., Liu M., Sharma P. P., Tiwary C. S., Ma L., Zou X., Zhou X. D., Yakobson B. I., Lou L., Ajayan P. M., American Chemical Society, 2015, 9, 5364-5371.
54. Shinagawa T., Garcia-Esparaza A. T., Takanabe K., Sci. Rep., 2015, doi: 10.1038/srep13801.
55. Ramos J. M., Dimeglio J. L., Rosenthal J., J. Am. Chem. Soc, 2014, 136, 8361-8367.